Sensors and Actuators B 253 (2017) 1152–1162

Contents lists available at ScienceDirect

Sensors and Actuators B: Chemical

journal homepage: www.elsevier.com/locate/snb

The design of excellent xylene gas sensor using Sn-doped NiO hierarchical nanostructure

Hongyu Gao[b], Dongdong Wei[b], Pengfei Lin[b], Chang Liu[b], Peng Sun[b,*], Kengo Shimanoe[c], Noboru Yamazoe[c], Geyu Lu[a,b,*]

[a] State Key Laboratory of Automotive Simulation and Control, Jilin University, 5988 Renmin Avenue, Changchun 130012, China
[b] State Key Laboratory on Integrated Optoelectronics, College of Electronic Science and Engineering, Jilin University, 2699 Qianjin Street, Changchun 130012, China
[c] Department of Energy and Material Sciences, Faculty of Engineering Sciences, Kyushu University, Kasuga-shi, Fukuoka 816-8580, Japan

ARTICLE INFO

Article history:
Received 20 March 2017
Received in revised form 5 June 2017
Accepted 28 June 2017
Available online 29 June 2017

Keywords:
Sn-doped NiO
Hierarchical nanostructure
Xylene
Gas sensor

ABSTRACT

A simple hydrothermal route to the synthesis of Sn-doped NiO hierarchical nanostructure is described in this paper. Gas sensors were fabricated from the as-prepared NiO nanostructures, and their gas sensing properties were investigated for response to various target gases. The results indicated that the sensor based on 3.0 at.% Sn-doped NiO nanospheres showed superior selectivity toward xylene, giving a response of 20.2–100 ppm, which was 12 times higher than that of the undoped NiO nanospheres. Moreover, this sensor based on the 3.0 at.% Sn-doped NiO hierarchical nanostructure had ppb-level detection limit that the response to 0.3 ppm xylene was 1.2. The likely reason for the improved sensing properties is the change of carrier concentration and chemisorbed oxygen amount caused by the implantation of Sn ions in NiO nanostructures.

1. Introduction

Xylene, which can be released from building materials, decorating materials, wood furniture, and carpets, is one of the representative pollutants among volatile organic compounds (VOCs) in the indoor environment. As we all know, it not only causes environmental pollution but also directly threats human health. Although its toxicity and hazard, xylene is still used in industries as intermediates to produce other chemicals and in research laboratories as solvents. Therefore, it is necessary to develop xylene gas sensors with good selectivity and high sensitivity.

Since Seiyama found that the conductance of ZnO thin films would change in different atmospheres [1], metal oxide semiconductor-based gas sensors have attracted extensive attention due to their high sensitivity, fast response/recovery time, low detection limit, low cost, and simplicity of fabrication [2–4]. In recent years, in order to meet the requirements in many areas, such as environment, medicine, and safety, extensive efforts on oxide semiconductor gas sensors have been focused on enhancing their sensitivity, selectivity, and stability. Specially, design and preparation of nanostructured oxides with various morphologies can effectively improve the sensing properties due to their high surface area [5–12]. However, the excellent results demonstrated in the literatures are obviously far from the growing need of the gas sensing performance. Actually for oxide semiconductor-based gas sensors, the widely accepted theory of sensing mechanism is that the reactions between the surface reactive chemical species such as O_2^-, O^-, O^{2-} and the gas molecules induce the change in resistance of oxide semiconductors [13–15]. On the basis of their sensing mechanism, the control of carrier concentration by doping may be a promising approach to significantly improve the gas sensing performance [16].

Nickel oxide (NiO), which is known as an important p-type metal oxide semiconductor, is widely used in the following fields such as energy storage [17], lithium ion batteries [18], catalysts [19], and sensors [16,20] owing to its steady chemical and electrical properties. Investigations into NiO nanostructures sensing properties have indicated that its sensitivity is relatively lower compared with that of some *n*-type metal oxide semiconductors [21–23]. Nevertheless, NiO has been found to have outstanding catalytic activity during the oxidation of volatile organic compounds (VOCs) [24]. In this regard, many studies have been conducted in order to improve the sensing performance of NiO gas sensors. Indeed, doping of NiO with aliovalent metal ions has been found to result in

* Corresponding authors at: State Key Laboratory on Integrated Optoelectronics, College of Electronic Science and Engineering, Jilin University, 2699 Qianjin Street, Changchun 130012, China
E-mail addresses: pengsun@jlu.edu.cn (P. Sun), lugy@jlu.edu.cn (G. Lu).

http://dx.doi.org/10.1016/j.snb.2017.06.177
0925-4005/

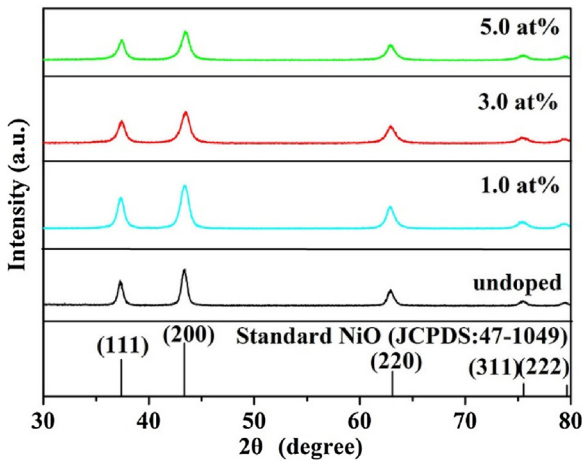

Fig. 1. XRD patterns of the pure, 1.0 at.%, 3.0 at.%, and 5.0 at.% Sn-doped NiO flower-like nanospheres.

improved gas sensing properties during sensing. For example, sensors based on Fe-doped NiO hollow spheres showed high response to 100 ppm C_2H_5OH at 350 °C that the value (R_g/R_a = 172.5) was about 31.4 times higher than that of undoped NiO hollow spheres (R_g/R_a = 5.5) [16]. Moreover, the gas sensor based on 3.0 wt% Cd-doped NiO showed excellent sensitivity toward 0.1% ethanol at the relatively low operating temperature of 100 °C [25]. It could be found that not only was the response increased, but also the operating temperature was decreased via the doping of NiO with aliovalent metal ions, both of which would improve the sensing performance.

In this work, a facile hydrothermal synthesis method was used to prepare pure and Sn-doped NiO hierarchical nanostructures. The resulting powders were applied to fabricate gas sensor devices which were then tested for sensitivity to a variety of gases. According to the tested data, the sensors using 3.0 at.% Sn-doped NiO nanospheres showed remarkable selectivity toward xylene and they were observably more sensitive to xylene compared with previously reported NiO sensor devices.

2. Experimental

2.1. Preparation of the pure and Sn-doped NiO flower-like nanospheres

The pure NiO flower-like nanospheres were prepared by a hydrothermal reaction. All the chemical reagents used in this experiment were analytical grade and used as received without further purification. Briefly, 2 mmol of $NiCl_2{\cdot}6H_2O$, different amounts of $SnCl_4{\cdot}5H_2O$ (the molar ratios of Sn/Ni were 0.0 at.%, 1.0 at.%, 3.0 at.%, and 5.0 at.%, respectively), and 2 mmol of hexamethylenetetramine (HMT) were dissolved into 30 mL of deionized water under vigorous stirring to form a homogeneous green solution. Five minutes later, dropping 2 mL of ethanolamine into the mixed solution, after stirring for several minutes, the mixed blue solution was transferred into a Teflon-lined stainless steel autoclave and heated at 160 °C for 12 h. After cooling down to room temperature, the resulting precipitates were centrifuged and washed with deionized water and ethanol several times and then dried at 80 °C for 24 h. Finally, the undoped and Sn-doped NiO flower-like nanospheres were obtained by annealing above precipitates at 400 °C for 2 h in air [26–29].

2.2. Characterization

X-ray diffraction (XRD) on a Rigaku TTRIII X-ray diffractometer (using Cu-Kα radiation with a wavelength of 1.5406 Å) was used to explore the crystalline structures of prepared materials. The data were collected over the 2θ range from 20° to 80° with a step rate of 10°/min. JSM-7500F (JEOL) field emission scanning electron microscope (FESEM) with an operating voltage of 15 kV was used to observe the morphology and microstructure of sam-

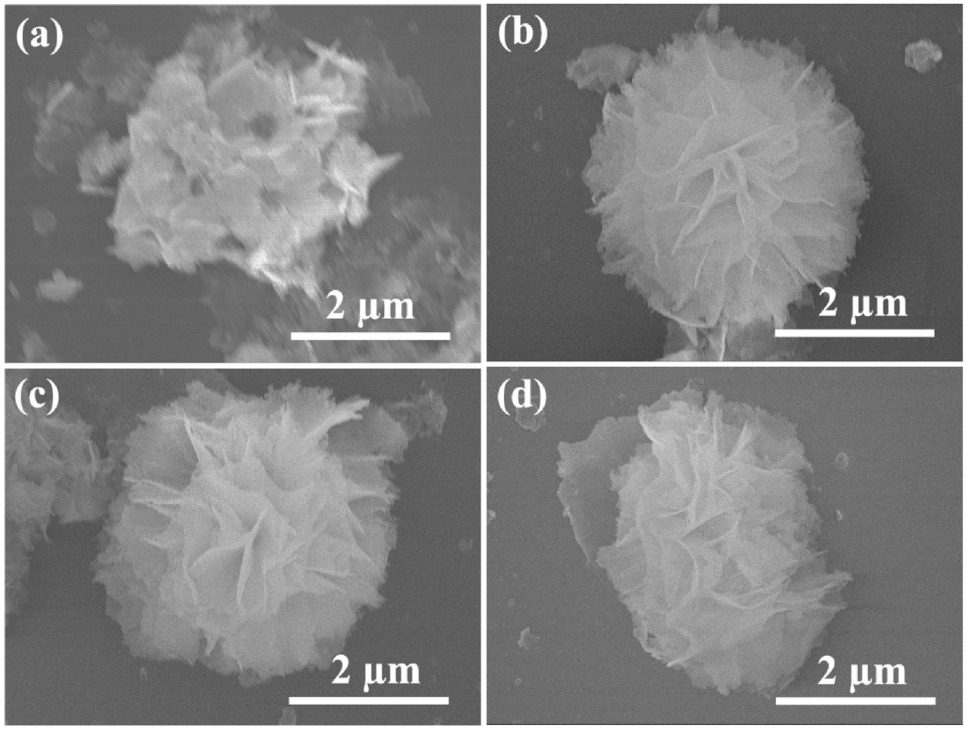

Fig. 2. FESEM images of the single (a) undoped, (b) 1.0 at.%, (c) 3.0 at.%, and (d) 5.0 at.% Sn-doped NiO hierarchical flower-like nanosphere.

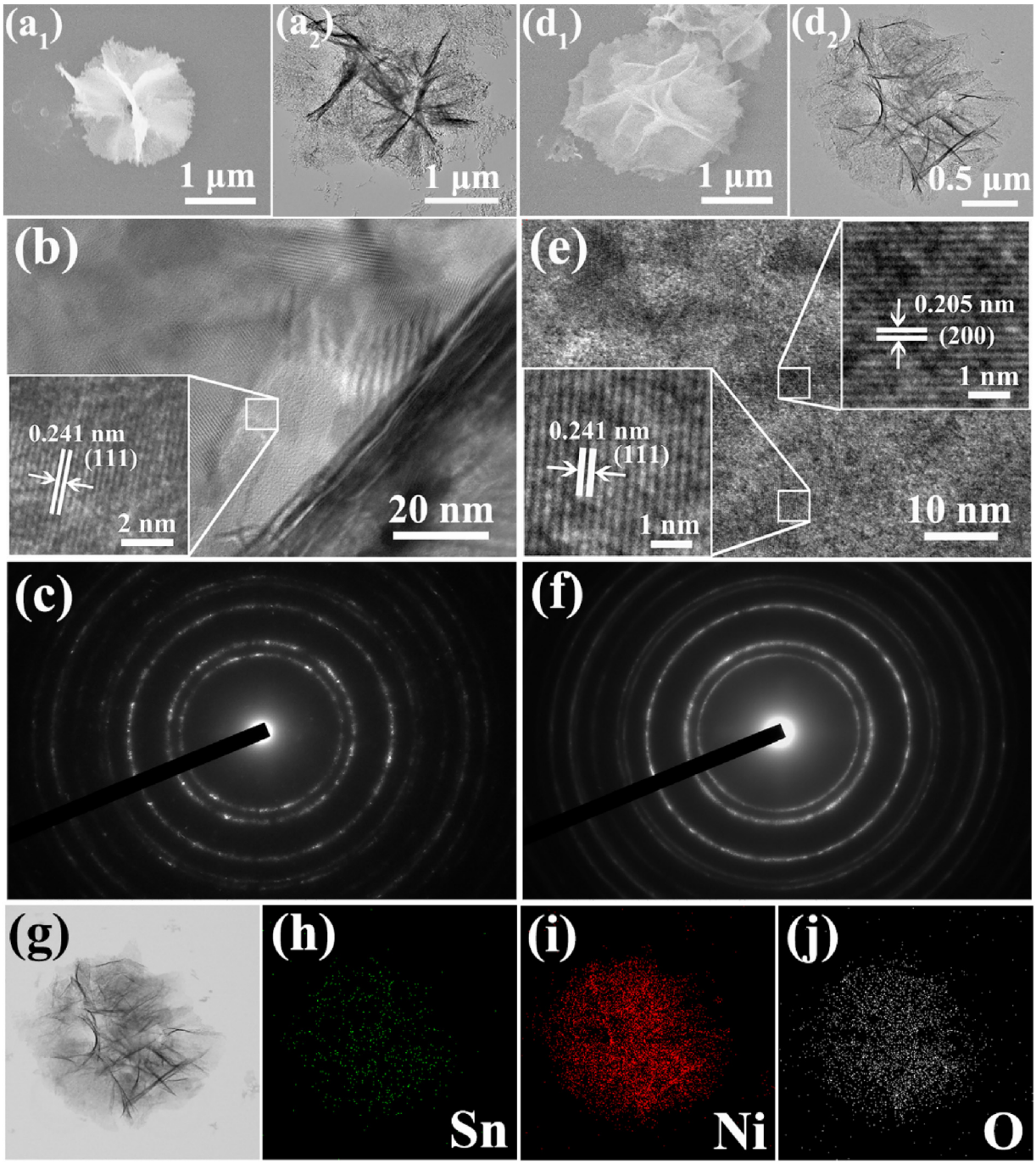

Fig. 3. (a_1, a_2, b and c) SEM, TEM, HRTEM and corresponding SAED pattern of the pure NiO sample. (d_1, d_2, e and f) SEM, TEM, HRTEM and corresponding SAED pattern of the 3.0 at.% Sn-doped NiO sample. (g, h, i and j) Scanning TEM (STEM) image and the corresponding energy dispersive X-ray spectroscopic (EDS) elemental mapping images of the 3.0 at.% Sn-doped NiO sample.

ples. The specific surface area was calculated from the BET equation with the help of Micromeritics Gemini VII apparatus (Surface Area and Porosity System). Transmission electron microscopy (TEM) and high-resolution TEM images were obtained from a JEM-2200FS (JEOL) transmission electron microscope under the operating voltage of 200 kV. The elemental mapping and spectrum of energy dispersive X-ray spectroscopic (EDS) were obtained from the TEM attachment. The X-ray photoelectron spectroscopy (XPS) measurements were operated with the source of Mg-Kα X-ray (1253.6 eV Specs XR50). A static test system was used to test gas sensing properties of the gas sensors under the laboratory condition (50% relative humidity, 25 °C). The system is cheap and easy-operating, it is made up of four parts: A constant-current power (Gwinstek GPD-3303S) providing different working temperatures to the sensors; An airtight chamber separating out a close space, where the gas can be changed by an air pump; A Fluke 8846a (Fluke Co.) recording the resistance of the sensors; A computer which can display and save the test data.

2.3. Fabrication and measurement of gas sensor

The fabrication of the gas sensor is described as following: The NiO nanosphere slurry was coated on an alumina tube with a pair of Au electrodes to form a thick film. Then the sensing devices were

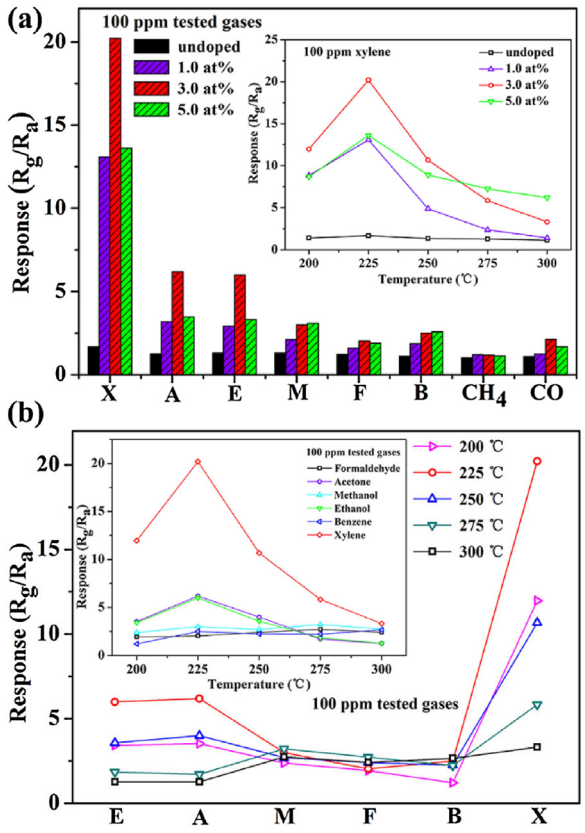

Fig. 4. (a) Gas responses of the sensors based on the pure, 1.0 at.%, 3.0 at.%, and 5.0 at.% Sn-doped NiO samples vs operating temperatures to 100 ppm xylene and responses of four sensors to 100 ppm eight target gases (X, xylene; A, acetone; E, ethanol; M, methanol; F, formaldehyde; B, benzene) at 225 °C. **(b)** Gas responses of the sensor based on the 3.0 at.% Sn-doped NiO sample to 100 ppm six target gases (E, ethanol; A, acetone; M, methanol; F, formaldehyde; B, benzene; X, xylene) at different operating temperatures.

Table 1
Textural parameters of the four as-obtained materials.

Samples	BET surface area ($m^2\ g^{-1}$)	Pore Volume ($cm^3\ g^{-1}$)	Average pore size (nm)
undoped	45.9	0.36	35.1
1.0 at.%	70.8	0.75	38.4
3.0 at.%	90.2	1.19	47.1
5.0 at.%	77.2	0.78	36.4

fired at 400 °C for 2 h in air using a muffle furnace. The details of the sensor fabrication have been described in our previous study [30]. The gas sensing performance of the gas sensor was measured by a static test system which could record real-time change in resistance of sensor. Firstly, the gas sensor was placed in an airtight chamber (1 L in volume) filled with fresh air. Then a certain volume of test gases was injected into the airtight chamber by a micro-injector for the investigation of the sensing performance. The gas response of the sensor was defined as R_g/R_a (p-type gas sensor), namely the ratio of the sensor resistance in target gases (R_g) to that of in air (R_a).

3. Results and discussion

3.1. Structural and morphological characteristics

The XRD patterns of the undoped and Sn-doped NiO samples are shown in Fig. 1 and confirm the formation of the face-centered cubic phase of NiO (JCPDS No. 47-1049). No other peaks which derived

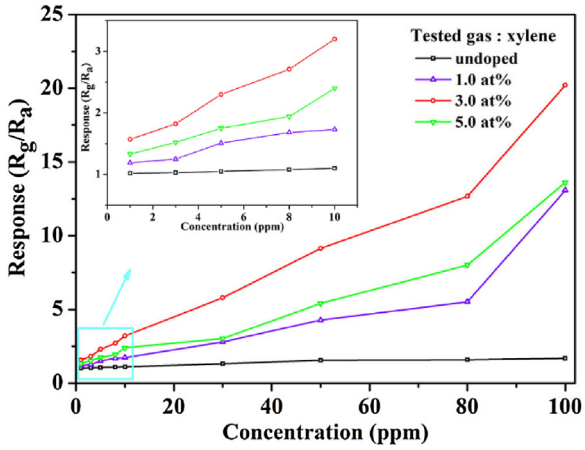

Fig. 5. Gas responses of four sensors as a function of the xylene concentration at 225 °C.

from the tetragonal rutile phase of SnO_2 or impurity phases were observed in the 1.0 at.%, 3.0 at.%, and 5.0 at.% Sn-doped NiO hierarchical nanospheres. This result indicated that the Sn ions were most likely incorporated into the NiO crystal lattice. Moreover, the peaks were obviously broadened, showing a small crystallite size. Using the Scherrer equation ($D = 0.89\lambda/\beta\cos\theta$, where D is the domain size, λ is the wavelength of the incoming radiation, β is the line broadening at full width half-maximum, and θ is the Bragg angle of the peak) to calculate the crystallite sizes for the as-prepared powders including pure, 1.0 at.%, 3.0 at.%, and 5.0 at.% Sn-doped NiO, indicating crystallite sizes of 14.1, 10.9, 10.3 and 9.7 nm, respectively.

The morphologies of the as-prepared Sn-doped NiO samples were examined by FESEM and TEM. As the high-magnification FESEM images of single nanosphere shown in Fig. 2, the NiO nanospheres were about 4 μm in diameter clearly, and it could also be observed that the flower-like NiO nanosphere was assembled from many curving and porous two-dimensional nanosheets. The panoramic SEM images of as-prepared samples are shown in Fig. S1. It could be found that the flower-like NiO nanospheres had relatively good dispersivity.

In addition, TEM images of undoped (a_2, b and c) and 3.0 at.% Sn-doped (d_2, e and f) NiO flower-like nanospheres are shown in Fig. 3. Image in Fig. 3a_2 further demonstrated that the NiO flower-like nanosphere appeared to have a hierarchical architecture, which was similar to the SEM observation (Fig. 3a_1). The HRTEM image of a single nanosheet shown in Fig. 3b displayed clear lattice fringes. And the lattice spacing (distance of two adjacent lattice fringes) was about 0.241 nm, which could correspond with the (111) lattice planes of NiO. The selected area electron diffraction (SAED) pattern is displayed in Fig. 3c, where a series of concentric diffraction rings could be observed. This observation indicated that the NiO nanosheet was polycrystalline. The 3.0 at.% Sn-doped NiO nanosphere was also analyzed by FESEM and TEM, images of which are shown in Fig. 3d_1, d_2, e. It could be found that the introduction of Sn ions rarely led to the changes in the morphology and microstructure. The HRTEM image of the 3.0 at.% Sn-doped NiO nanosheet showed clear lattice fringes with spacing of 0.205 and 0.241 nm, which could be attributed to the (200) and (111) lattice planes of NiO, respectively. Furthermore, the EDS elemental mapping analysis was carried out on the 3.0 at.% Sn-doped NiO flower-like nanospheres as shown in Fig. 3h-j, depicting the spatial distribution of Sn, Ni, and O, respectively. Obviously, all three kinds of elements were detected and distributed uniformly in the region of flower-like nanospheres. Furthermore, the signals of Ni and O were much stronger than that of Sn, which indicated that the content of Sn was much lower than that of Ni and O.

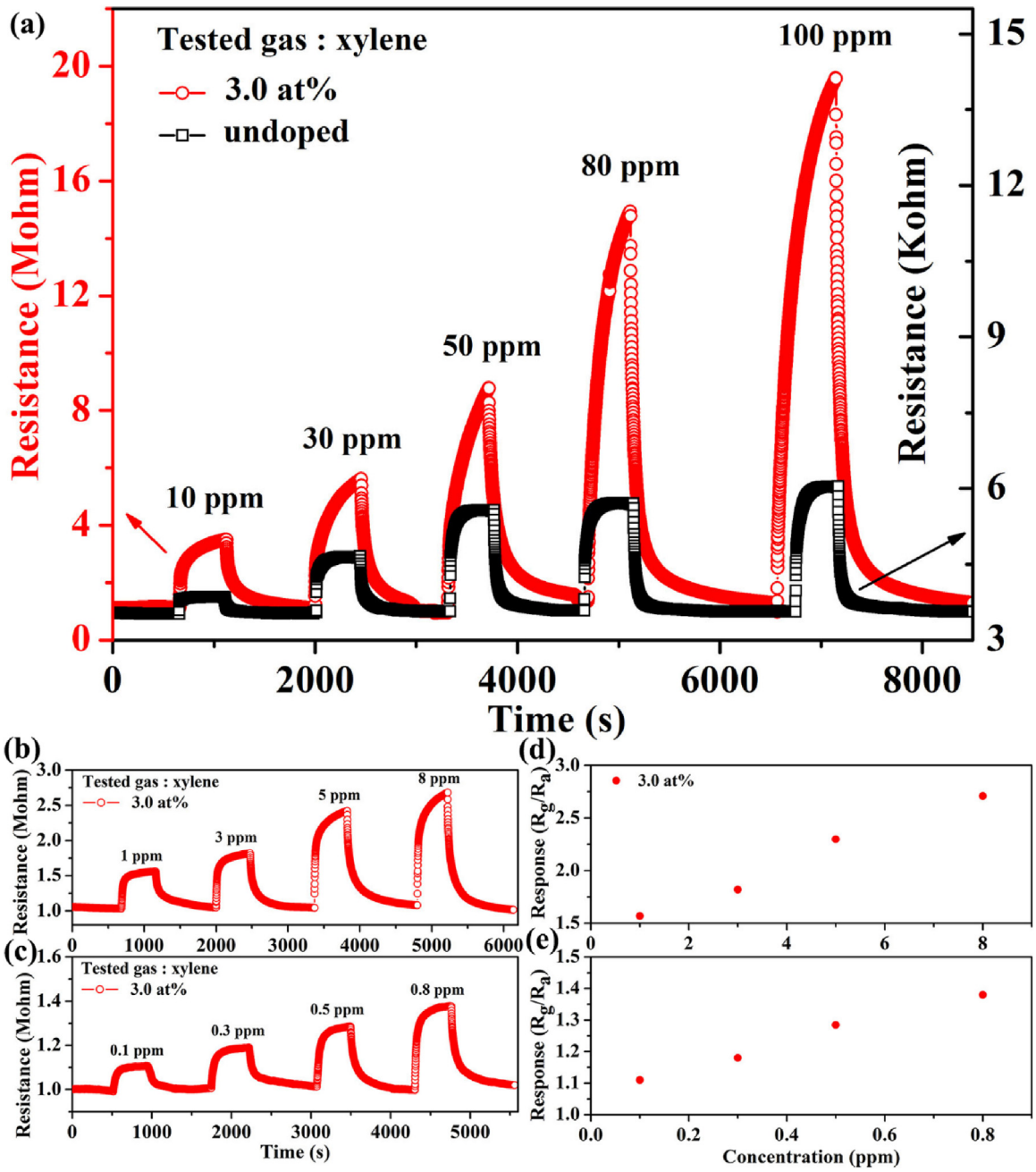

Fig. 6. (a) Dynamical response-recovery curves of the 3.0 at.% Sn-doped NiO and pure NiO flower-like nanospheres to different concentrations of xylene from 10 to 100 ppm. (b, c) Dynamical response-recovery curves of the 3.0 at.% Sn-doped NiO nanospheres to low concentrations of xylene from 1 to 8 ppm and 0.1–0.8 ppm respectively at 225 °C. (d, e) Gas responses of the sensor based on the 3.0 at.% Sn-doped NiO sample to low concentrations of xylene from 1 to 8 ppm and 0.1–0.8 ppm respectively at 225 °C.

3.2. Gas sensing characteristics

In order to examine the effect of the Sn doping on the gas sensing properties of the NiO nanospheres, the gas sensing performance of the sensors based on the undoped and different amounts of Sn-doped NiO samples was investigated. First of all, in order to explore the optimal operating temperature and Sn doping amount, the responses of gas sensors based on the pure, 1.0 at.%, 3.0 at.%, and 5.0 at.% Sn-doped NiO samples to 100 ppm xylene were measured at different operating temperatures from 200 to 300 °C.

As shown in Fig. 4a (inset), the curve showed the correlation between gas response and operating temperature for all the samples, clearly, the optimal operating temperature of all the samples was 225 °C. Obviously, significant improvements in gas responses were observed for all the sensors based on Sn-doped NiO. Among them, the responses of the sensors based on the pure, and 3.0 at.% Sn-doped NiO to 100 ppm xylene at 225 °C were 1.7, and 20.2, respectively. The results indicated that the sensor based on 3.0 at.% Sn-doped NiO showed the highest response to 100 ppm xylene and the value was about 12 times higher than that of pure NiO. Meanwhile, the selectivity curves shown in Fig. 4a describe the gas responses of pure and three Sn-doped sensors to 100 ppm of eight different target gases at 225 °C. The target gases are xylene, acetone, ethanol, methanol, formaldehyde, benzene, CH_4, and CO respectively. Clearly, in comparison with the pure NiO, all the Sn-doped NiO samples exhibited enhanced response for each test gas. Additionally, the responses of all the sensors to xylene were visibly higher than that to other gases. Especially, the sensor based

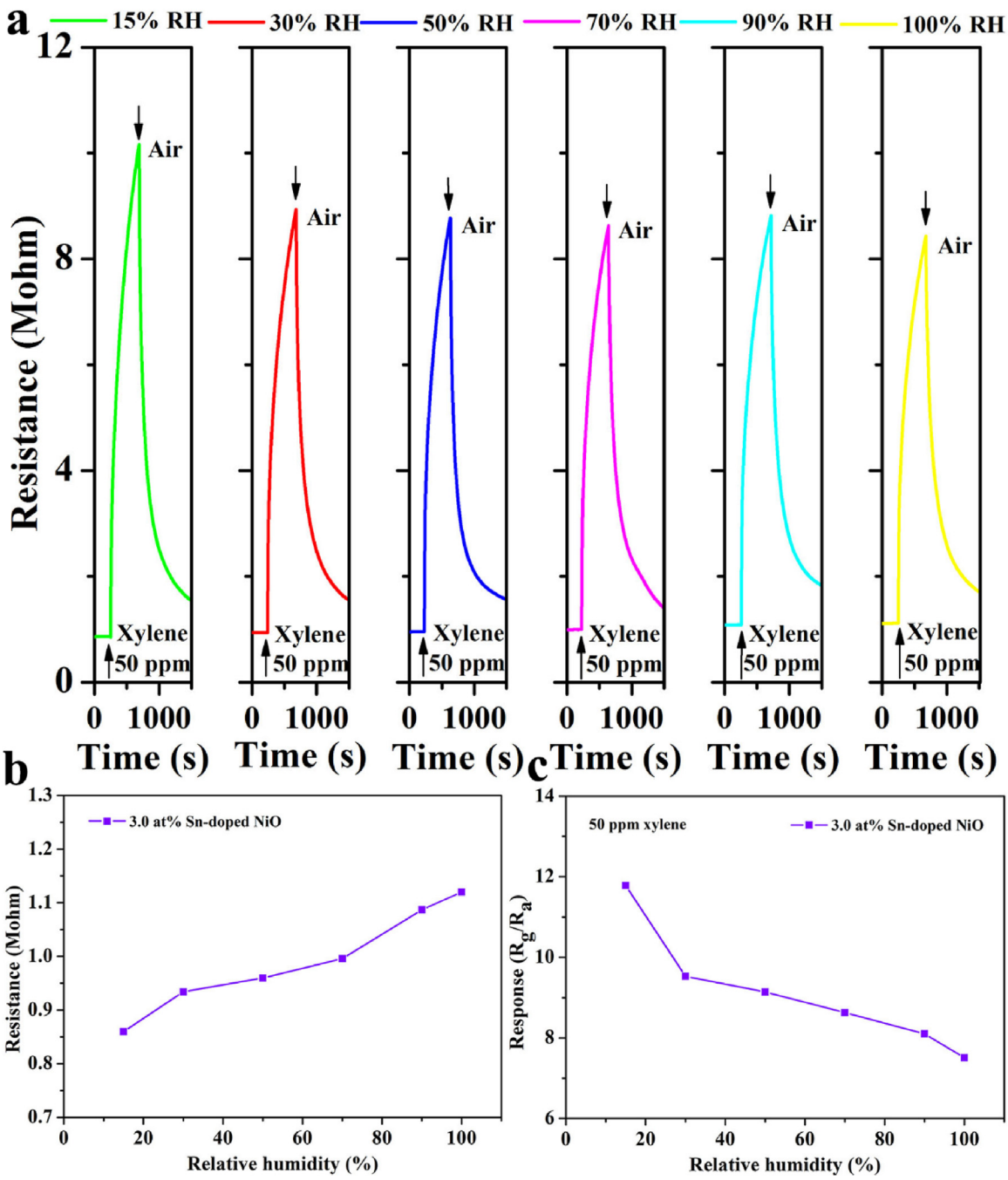

Fig. 7. (a) Dynamic response curves of 3.0 at.% Sn-doped NiO sensor to 50 ppm xylene in different humidity (15%-100% RH) at 225 °C. (b, c) Corresponding values of initial resistances in air and gas responses to 50 ppm xylene at the increasing humidity, respectively.

on 3.0 at.% Sn-doped NiO had the highest response to xylene and the value was about 3.3-17.1 times higher than that to other target gases, while the ratio was only about 1.3–1.6 for the pure NiO. According to the study of the gas-sensing selectivity mechanism [31], both the amount of gas adsorption and LUMO (lowest unoccupied molecule orbit) energy have impacts on selectivity of the sensor. Thus, owing to the different amount of gas adsorption and LUMO energy of various target gases, the gas responses will be different from each other and exhibit selectivity. Herein, the reason for the high response to xylene of the NiO gas sensors were also talked about. On the basis of the reported literature [32], the responses of the pure NiO are negligibly low, however, NiO is a good catalyst for promoting the adsorption of methyl radicals and oxidizing xylene, which could significantly enhanced the gas response to xylene after using an appropriate modification method. Of course, these analyses above are based on the existing literatures, and further studies are necessary in order to give out essential and universal theories on the gas-sensing mechanism.

Actually, in the practical use, gas sensors are always work at the complex environments surrounded by various kinds of gases. Therefore, good selectivity of sensors to target gases is one of the key parameters as well. So further investigation for selectivity was conducted. For the comprehensive and accurate selectivity assessment of the sensor, the selectivity curves of the sensor based on the 3.0 at.% Sn-doped NiO towards six VOCs (ethanol, acetone, methanol, formaldehyde, benzene, xylene) at different operating temperatures (200, 225, 250, 275, 300 °C) are shown in Fig. 4b, which demonstrates the optimum working temperature of each

Table 2
Comparison of xylene sensing performance among gas sensors based on different sensing materials.

Materials	T (°C) & RH (%)	Conc. (ppm)	R_g/R_a or R_a/R_g	Res. & Recov. time (s)	LOD (ppm)	Improved ratio	Ref.
0.6 at.% Pd-doped $WO_3 \cdot H_2O$	230 & –	10	21	~1 & ~2	0.1	3.3	[34]
		200	55.5	–		3.8	
5 at.% Cr-doped	139 & 43	5	6.4	15–30 & 10–30	1.15	4.9	[35]
Co_3O_4		100	~18.6	–		~9.3	
5 wt% Fe-doped MoO_3	206 & 40	100	6.1	20 & 75	~5	2.1	[36]
2.04 wt% Au-loaded α-MoO_3	250 & –	5	2.5	118 & 289	0.5	–	[37]
		100	22.1	–		3.9	
α-MoO_3/α-Fe_2O_3	206 & –	5	4.8	–	–	3	[38]
		100	6.8	87 & 190		~2.3	
2 at.% Ni-doped TiO_2	302 & –	100	4.4	9 & 1.2	–	2.4	[39]
0.4 wt% Co-doped ZnO	320 & 25	100	14.8	4 & 6	–	3.4	[40]
Zn-W-O nanocomposite	420 & –	100	7.1	–	–	~3.5	[41]
$Cr_2O_3/ZnCr_2O_4$ nanocomposite	275 & –	5	69.2	–	0.25	16.5	[42]
1.15 at.% Cr-doped NiO	400 & –	5	11.6	–	0.25	~5.8	[43]
2 at.% W-doped NiO	375 & 25–35	200	8.7	178 & 152	~15	3.3	[44]
3 at.% Sn-doped NiO	225 & 50	100	20.2	298 & 223	0.3	12	This work

LOD: limit of detection.
Improved ratio: the ratio of responses between the well-modified sensor and the untreated sensor in the same test condition.

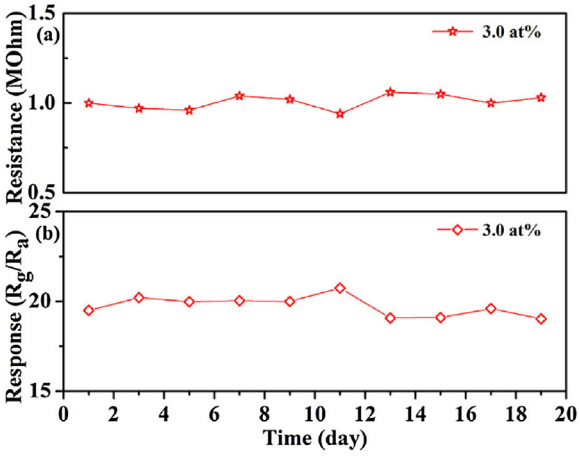

Fig. 8. (a) Resistances in air and (b) responses to 100 ppm xylene of the sensor based on the 3.0 at.% Sn-doped NiO as a function of the test days at 225 °C.

target gas. Moreover the optimum target gas at each operating temperature could be found obviously from another form of selectivity curves shown in the inset of Fig. 4b. It could be noticed that the sensor based on the 3.0 at.% Sn-doped NiO had a good selectivity towards xylene at the temperature between 200 °C–300 °C, and the optimum working temperature is 225 °C.

Fig. 5 shows the responses of four gas sensors to xylene with various concentrations at 225 °C. It could be observed that the gas responses increased with increasing xylene concentration from 1 to 100 ppm for all the sensors. Among them, the response of the sensor based on the 3.0 at.% Sn-doped NiO was apparently higher than that of other gas sensors. And the inserted picture shows the curves of response of four gas sensors to xylene in low concentration from 1 to 10 ppm. The sensor based on the 3.0 at.% Sn-doped NiO displayed excellent linear responses to relatively low concentrations of xylene.

Moreover, the dynamical response-recovery curves of two sensors based on pure and 3.0 at.% Sn-doped NiO to different xylene concentrations (10–100 ppm) at 225 °C are displayed in Fig. 6a. In addition, dynamical response-recovery curves of sensor based on 3.0 at.% Sn-doped NiO to low xylene concentration (1–8 ppm and 0.1–0.8 ppm) at 225 °C are displayed in Fig. 6b and c respectively and their corresponding values of response are shown in Fig. 6d and e. For the sensors, the resistances increased upon exposure to xylene, which were the same gas sensing behaviors as p-type oxide semiconductors. Besides, the sensors showed outstanding response and recovery characteristics toward different concentration of xylene. For the response curves of the sensor based on 3.0 at.% Sn-doped NiO, the corresponding responses had a significant enhancement with the increasing concentration of xylene and the sensor had an obvious response to 0.3 ppm xylene (the response to 0.3 ppm xylene was 1.2), which indicated that the sensor based on the 3.0 at.% Sn-doped NiO hierarchical flower-like nanospheres had ppb-level detection limit.

As shown in Fig. 7, the interferential effect of water vapor on the response and resistance was investigated. Six real-time response curves to 50 ppm xylene at 225 °C in different humidity condition (15%, 30%, 50%, 70%, 90% and 100% RH) are shown in Fig. 7a and corresponding values of resistance and response are shown in Fig. 7b and c, respectively. Apparently, high relative humidity (RH) had some influence on the sensing properties, the resistance in air at 225 °C increased with the increasing RH, while the response toward 50 ppm xylene at 225 °C decreased. The reason for this phenomenon could be searched in the reported literature [33]. First, reaction between water and adsorbed oxygen decreased the band bending, resulting in the increase of resistance; second, oxygen ions near the NiO surface were competed by target gas and water vapors, which decreased the effect of target gas exposure and lower the gas response.

Response and recovery times toward 100 ppm xylene at 225 °C of the 3.0 at.% Sn-doped NiO gas sensor are shown in Fig. S2a, showing the response and recovery times of 298 and 223s, respectively. And five shark-fin-like cyclic resistant curves of the sensor based on the 3.0 at.% Sn-doped NiO to 100 ppm of xylene at 225 °C are shown in Fig. S2b. It could be found that there was no obvious floating in responses during the periods of cycle measurement. The gas response was rapid, and a shark-fin-like profile was reached within minutes of exposure to xylene. When the xylene flow was stopped, the response dropped to the baseline again. Those results above demonstrated a good repeatability of the sensor. Moreover, as shown in Fig. 8, the resistance in air and corresponding gas response to 100 ppm xylene at 225 °C were nearly constant in the 20 test days, which indicated the long-term stability of the sensor based on the 3.0 at.% Sn-doped NiO sample.

In a word, on the basis of the preceding paragraphs, we can draw the conclusion that the doping of Sn into NiO has an effect on promoting the gas sensing properties of the NiO-based gas sensor and the optimum doping amount of Sn was considered to be 3.0 at.%.

Herein, xylene sensing properties of the 3.0% Sn-doped NiO sensor in this study and some reported gas sensors based on various sensing materials are summarized in Table 2 [34–44]. It is apparent

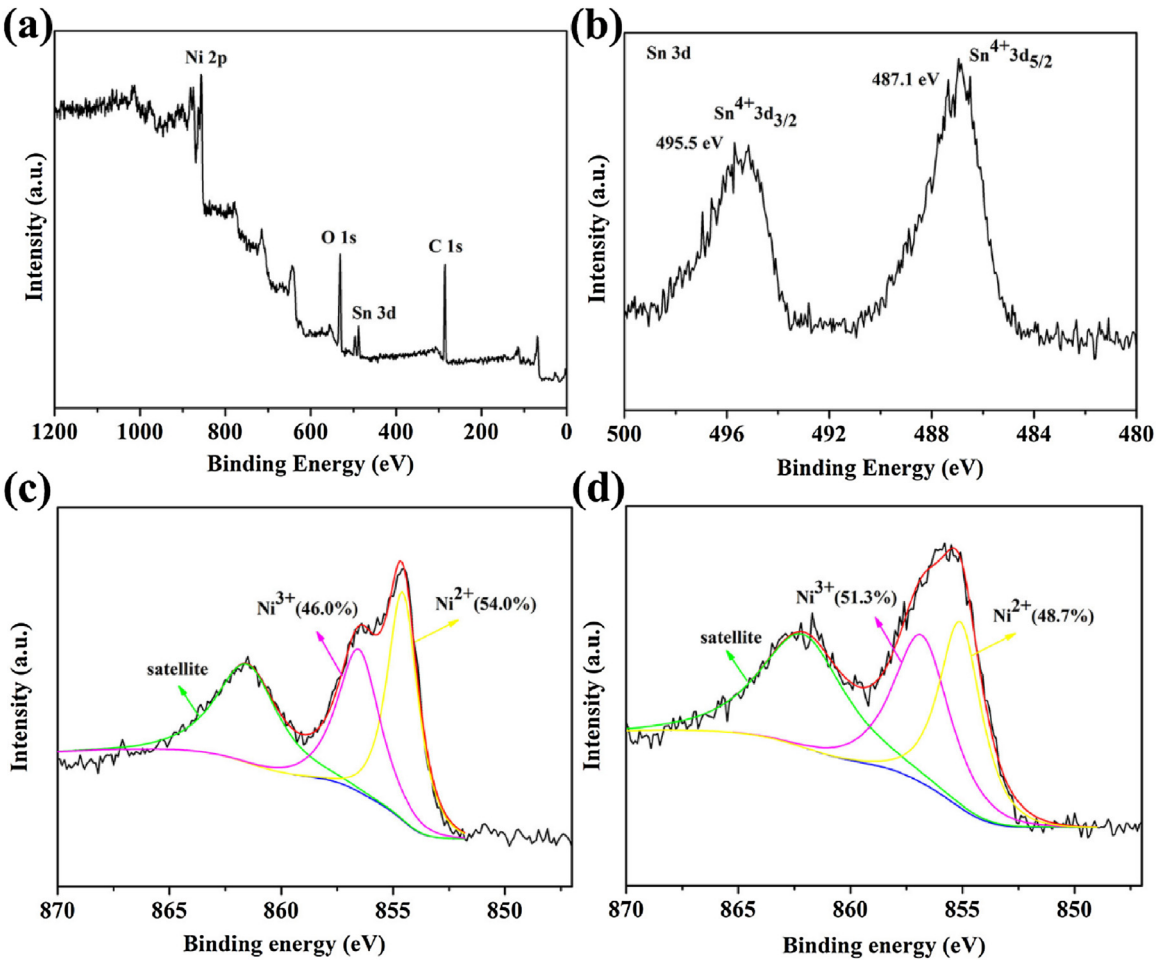

Fig. 9. XPS (a) survey scan and (b) Sn 3d spectra of the 3.0 at.% Sn-doped NiO flower-like nanospheres. Ni $2p_{3/2}$ XPS spectra of the (c) pure and (d) 3.0 at.% Sn-doped NiO flower-like nanospheres.

that these xylene gas sensors are mainly fabricated from modified WO_3, MoO_3, α-Fe_2O_3, TiO_2, ZnO, Cr_2O_3, Co_3O_4, NiO materials or some composites. And on the whole, gas sensors based on p-type semiconductors showed larger lifting space (improved ratio) on the sensing properties than that of the n-type semiconductor gas sensors, because of the relatively poorer gas sensing performance of the untreated p-type semiconductors (especially for pure NiO) compared with that of the untreated n-type semiconductors. As for the specific gas sensor, though the response and recover times were relatively longer, the 3 at.% Sn-doped NiO gas sensor in this work not only gave out a high ratio of gas-sensing improvement but also exhibited good sensing properties, such as higher response, lower working temperature, lower detection limit and better humidity independence. Additionally, some gas responses of sensors [36,39,41,44] were relatively low, some responses of the sensors [34,38] were less increased with the obviously increased xylene concentration indicating relatively low saturation concentrations, and some sensors [42,43] showed much higher responses to 5 ppm xylene, but did not exhibited matched low detection limits expectantly. So, compared with these sensors above, the 3 at.% Sn-doped NiO gas sensor also exhibited a wider detection range of xylene and better linear relation between gas response and concentration.

3.3. Gas sensing mechanism

As for the gas sensing mechanism of oxide semiconductors, the most widely accepted theory is that the electrical conductivity and the surface chemisorbed oxygen species of the sensing materials have a primary effect on the gas sensing properties. Generally, when the gas sensor based on NiO nanostructures is exposed to air, oxygen molecules will be adsorbed on the surface of NiO and go on to be ionized by electrons derived from the conduction band to form species, which leads to the formation of a hole accumulation layer. Since the majority carrier in NiO is hole, so the resistance of NiO will get decreased. On exposure to a reducing gas, the target gas will react with chemisorbed oxygen ions, resulting in the release of electrons back into the conduction band of NiO. So in this way, the accumulation layer get thinner, which causes the increase of the sensor resistance.

The ability of the sensing material to adsorb and ionize oxygen species is fundamental to the sensor performance. The enhanced performance observed here is likely to be the result of two factors. First, the crystallite size and the specific surface area were talked about. The average crystallite sizes of the pure, 1.0 at.%, 3.0 at.%, and 5.0 at.% Sn-doped NiO primary nanoparticles were calculated to be 14.1, 10.9, 10.3 and 9.7 nm, respectively. It could be found that the crystallite size decreased with the increase of Sn doping amount. Moreover it could reflect the change of grain (particle) size in some way and according to a previous sensing theory, reducing the particle size increases the sensitivity [45]. As for the specific surface area, the N_2 adsorption-desorption isotherms of the four as-obtained samples are shown in Fig. S3 and the measured results of textural parameters are listed in Table 1. The results of measurements showed the BET surface areas of pure NiO, 1.0 at.%, 3.0 at.%, and 5.0 at.% Sn-doped NiO flower-like nanospheres were 45.9, 70.8,

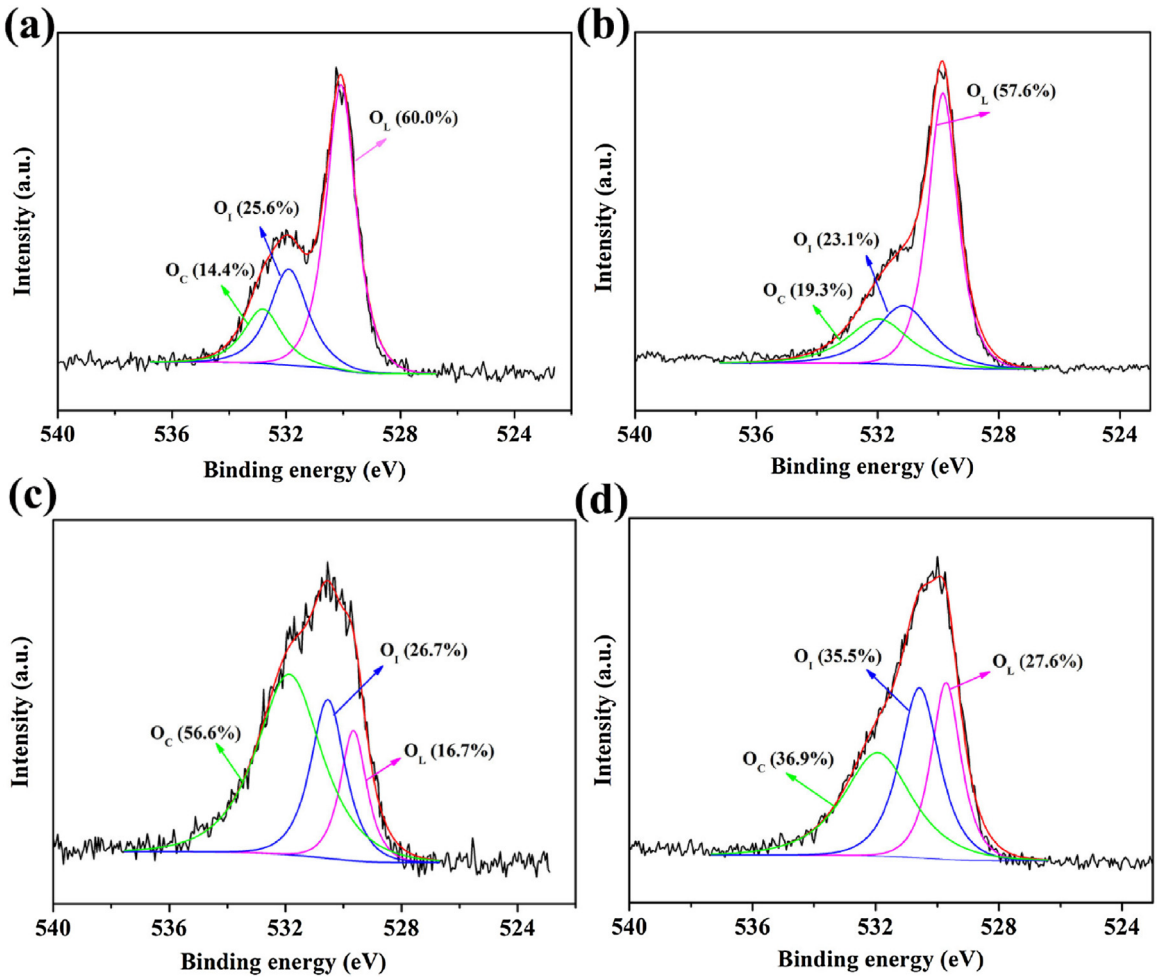

Fig. 10. O 1s XPS spectra of (a) pure, (b) 1.0 at.%, (c) 3.0 at.%, (d) 5.0 at.% Sn-doped NiO flower-like nanospheres, respectively.

90.2, and 77.2 $m^2 g^{-1}$, respectively. Obviously, the specific surface area of 3.0 at.% Sn-doped NiO nanospheres (90.2 $m^2 g^{-1}$) was larger than that of pure NiO (45.9 $m^2 g^{-1}$). Moreover, the other two parameters (pore volume and average pore size) of 3.0 at.% Sn-doped NiO nanospheres were superior to those of the undoped, 1.0 at.%, and 5.0 at.% Sn-doped NiO as well. These meant that more amount of oxygen could be adsorbed on the surface of NiO after doping Sn, and such porous hierarchical nanostructure could simplify gas diffusion to the interior of nanospheres, both of which could lead to the improvement in gas sensing properties. Though, it could be found that the BET surface area first increased when the Sn doping amount was not too high and then decreased, which was not matched with the changing tendency of average crystallite size. It meant that the crystallite size was not directly relevant to the specific surface area or the enhanced performance. Strictly speaking, crystallite size is different from the grain (particle) size and on the basis of the equation $S_w = K/\rho D$ [46], where S_w is the specific surface area, ρ is the bulk density, K is a shape factor (K = 6 for the spherical nanoparticles), D is the average particle size, it could be found easily that the specific surface area has close relation with the structure and morphology. Therefore, the decrease of specific surface area of the 5.0 at.% Sn-doped NiO may due to the too dense nanosheet-assembled nanoflowers [47]. Actually, the enhanced sensing performance results from the co-effect of multi-factor, the decrease of crystallite size and the increase of specific surface area may just partly explained the enhanced performance [45], therefore more factors need to be concerned for the enhanced sensing performance. Second, the investigation of carrier concentration and distribution of oxygen component in the pure and Sn-doped NiO was carried out by XPS analysis.

Fig. 9a shows the XPS survey spectrum of the 3.0 at.% Sn-doped NiO sample, in this picture, the signals of Ni, O and Sn could be clearly observed. As the Sn 3d spectrum illustrated in Fig. 9b, the two characteristic peaks located at 495.5 eV and 487.1 eV were assigned to Sn^{4+} [48]. Fig. 9c and d show the high resolution scans of the undoped and 3.0 at.% Sn-doped NiO flower-like nanospheres for Ni $2p_{3/2}$. From which, Ni^{2+} and Ni^{3+} bonding energies were clearly observed at 854.6 and 856.5 eV for the pure NiO, as well as 855.1 and 856.8 eV for the 3.0 at.% Sn-doped NiO. It could be found that the Ni^{3+}/Ni^{2+} ratio of NiO samples was increased after doping 3.0 at.% Sn into NiO crystal lattice. This indicates the partial of Ni^{2+} ions are oxidized to Ni^{3+} due to Sn doping. As reported in previous literatures, the adsorbed oxygen with negative charge on the surface of NiO can lead to the formation of Ni^{3+}, what's more, Ni^{3+} can also be formed by the negatively charged interstitial oxygen (O_i'') [49,50]. As shown in Eq. (1), substitution of Sn^{4+} at the site of Ni^{2+} can be described with the electronic compensation mechanism. And the oxygen molecules formed in Eq. (1) will be converted into negatively charged interstitial (or surface) oxygen as shown in Eq. (2), through the partial oxidation of Ni^{2+} into Ni^{3+} (Eq. (2)).

$$SnO_2 \xrightarrow{NiO} Sn_{Ni}^{\bullet\bullet} + 2e^{'} + O_O^{\times} + \frac{1}{2}O_2\,(g) \quad (1)$$

$$\frac{1}{2}O_2\,(g) + 2NiO \xrightarrow{2NiO} O_i^{''} + 2Ni_{Ni}^{\bullet} + 2O_O^{\times} \quad (2)$$

And in Eq. (1), electrons are generated owing to the substitution of Sn^{4+} at Ni^{2+} sites, which increases the resistance of NiO. It has been demonstrated that when the hole concentration become low, the same amounts of injected electrons produced in the sensing reaction between xylene molecules and chemisorbed oxygen ions will result in a higher variation in sensor resistance, which eventually leads to the enhanced gas response [51,52].

In addition, as shown in Fig. 10, the O 1s XPS peaks of the four NiO samples were asymmetric and could be fitted into three different components [53,54]. They were lattice oxygen (O_L), oxygen deficient regions (O_I), and chemisorbed oxygen species (O_C), located at the binding energies of about 529.8 ± 0.3 eV, 531.2 ± 0.7 eV, and 532.4 ± 0.4 eV respectively.

The relative percentages of O_L, O_I, and O_C components in the undoped NiO were approximately 60.0%, 25.6%, and 14.4%, while those were 16.7%, 26.7%, and 56.6% in the 3.0 at.% Sn-doped NiO. Obviously, the contents of O_I and O_C components were increased after Sn doping, which indicated that the deficient and chemisorbed oxygen in NiO sample had close relation to the gas sensing properties. Generally speaking, more active sites for the gas reaction could be provided as well as the adsorption on the surface of the sensing materials owing to the increase of O_I component. Moreover, the rise of O_C component meant that more surface chemisorbed oxygen species could participate in the oxidation-reduction reaction, causing a larger change in sensor resistance. Therefore, the improvement in gas response can be successfully achieved by adjusting the hole concentration and distribution of oxygen components using Sn doping strategy.

4. Conclusions

In summary, we have demonstrated that the pure, 1.0 at.%, 3.0 at.% and 5.0 at.% Sn-doped NiO flower-like nanospheres can directly be synthesized using a simple hydrothermal reaction. The pure and Sn-doped NiO were utilized in sensor devices and their gas sensing properties were examined. The results revealed that the sensor based on the 3.0 at.% Sn-doped NiO had the significantly enhanced gas response to xylene compared with that of the other sensors. The changes in crystallite size, specific surface area, and carrier concentration caused by Sn doping may be responsible for the improvement in sensing properties.

Acknowledgments

This work is supported by the National Key Research and Development Program (No. 2016YFC0207300). National Nature Science Foundation of China (Nos. 61503148, 61520106003, 61327804, 61374218) and Program for Chang Jiang Scholars and Innovative Research Team in University (No. IRT13018). National High-Tech Research and Development Program of China (863 Program, Nos. 2013AA030902 and 2014AA06A505). Science and Technology Development Program of Jilin Province (No. 20170520162JH). China Postdoctoral Science Foundation funded project No. 2015M580247.

Appendix A. Supplementary data

Supplementary data associated with this article can be found, in the online version, at http://dx.doi.org/10.1016/j.snb.2017.06.177.

References

[1] T. Seiyama, A. Kato, K. Fujush, M. Magatain, A new detector for gases component using semiconductor thin-film, Anal. Chem. 34 (1962) 1052–1053.
[2] S. Das, V. Jayaraman, SnO_2: a comprehensive review on structures and gas sensors, Prog. Mater. Sci. 66 (2014) 112–255.
[3] A. Afzal, N. Cioffi, L. Sabbatini, L. Torsi, NO_x sensors based on semiconducting metal oxide nanostructures: progress and perspectives, Sens. Actuators B 171–172 (2012) 25–42.
[4] G. Korotcenkov, Metal oxides for solid-state gas sensors: what determines our choice, Mater. Sci. Eng. B 139 (2007) 1–23.
[5] C.P. Gu, X.J. Xu, J.R. Huang, W.Z. Wang, Y.F. Sun, J.H. Liu, Porous flower-like SnO_2 nanostructures as sensitive gas sensors for volatile organic compounds detection, Sens. Actuators B 174 (2012) 31–38.
[6] J. Li, H.Q. Fan, X.H. Jia, Multilayered ZnO nanosheets with 3D porous architectures: synthesis and gas sensing application, J. Phys. Chem. C 114 (2010) 14684–14691.
[7] N.K. Singh, S. Shrivastava, S. Rath, S. Annapoorni, Optical and room temperature sensing properties of highly oxygen deficient flower-like ZnO nanostructures, Appl. Surf. Sci. 257 (2010) 1544–1549.
[8] H.Y. Lai, T.H. Chen, C.H. Chen, Architecture controlled synthesis of flower-like In_2O_3 nanobundles with significantly enhanced ultraviolet scattering and ethanol sensing, CrystEngComm 14 (2012) 5589–5595.
[9] Z.P. Li, Y.J. Fan, J.H. Zhan, In_2O_3 nanofibers and nanoribbons: preparation by electrospinning and their formaldehyde gas-sensing properties, Eur. J. Inorg. Chem. 21 (2010) 3348–3353.
[10] X.L. Hu, J.C. Yu, J.M. Gong, Q. Li, G. Li, α-Fe_2O_3 nanorings prepared by a microwave-assisted hydrothermal process and their sensing properties, Adv. Mater. 19 (2007) 2324–2329.
[11] G. Korotcenkov, The role of morphology and crystallographic structure of metal oxides in response of conductometric-type gas sensors, Mater. Sci. Eng. R 61 (2008) 1–39.
[12] J.H. Lee, Gas sensors using hierarchical and hollow oxide nanostructures: overview, Sens. Actuators B 140 (2009) 319–336.
[13] N. Yamazoe, G. Sakai, K. Shimanoe, Oxide semiconductor gas sensors, Catal. Surv. Asia 7 (2003) 63–75.
[14] Y. Shimizu, M. Egashira, Basic aspects and challenges of semiconductor gas sensors, MRS Bull. 24 (1999) 18–24.
[15] N. Barsan, D. Koziej, U. Weimar, Metal oxide-based gas sensor research: how to, Sens. Actuators B 121 (2007) 18–35.
[16] H.J. Kim, K.I. Choi, K.M. Kim, C.W. Na, J.H. Lee, Highly sensitive C_2H_5OH sensors using Fe-doped NiO hollow spheres, Sens. Actuators B 171–172 (2012) 1029–1037.
[17] M.X. Liu, X. Wang, D.Z. Zhu, L.C. Li, H. Duan, Z.J. Xu, Z.W. Wang, L.H. Gan, Encapsulation of NiO nanoparticles in mesoporous carbon nanospheres for advanced energy storage, Chem. Eng. J. 308 (2017) 240–247.
[18] X.B. Zhu, B. Luo, T. Butburee, J.W. Zhu, S. Han, L.Z. Wang, Hierarchical macro/mesoporous NiO as stable and fast-charging anode materials for lithium-ion batteries, Microporous Mesoporous Mater. 238 (2017) 78–83.
[19] W.X. Wei, X.H. Jiang, L.D. Lu, X.J. Yang, X. Wang, Study on the catalytic effect of NiO nanoparticles on the thermal decomposition of TEGDN/NC propellant, J. Hazard. Mater. 168 (2009) 838–842.
[20] X. Luo, Z.J. Zhang, Q.J. Wan, K.B. Wu, N.J. Yang, Lithium-doped NiO nanofibers for non-enzymatic glucose sensing, Electrochem. Commun. 61 (2015) 89–92.
[21] L.A. Patil, M.D. Shinde, A.R. Bari, V.V. Deo, Highly sensitive and quickly responding ultrasonically sprayed nanostructured SnO_2 thin films for hydrogen gas sensing, Sens. Actuators B 143 (2009) 270–277.
[22] Z.J. Li, Y.W. Huang, S.C. Zhang, W.M. Chen, Z. Kuang, D.Y. Ao, W. Liu, Y.Q. Fu, A fast response & recovery H_2S gas sensor based on α-Fe_2O_3 nanoparticles with ppb level detection, J. Hazard. Mater. 300 (2015) 167–174.
[23] A. Katoch, S.W. Choi, H.W. Kim, S.S. Kim, Highly sensitive and selective H_2 sensing by ZnO nanofibers and the underlying sensing mechanism, J. Hazard. Mater. 286 (2015) 229–235.
[24] G.M. Bai, H.X. Dai, J.G. Deng, Y.X. Liu, K.M. Ji, Porous NiO nanoflowers and nanourchins: high active catalysts for toluene combustion, Catal. Commun. 27 (2012) 148–153.
[25] M.B. Amor, A. Boukhachem, A. Labidi, K. Boubaker, M. Amlouk, Physical investigations on Cd doped NiO thin films along with ethanol sensing at relatively low temperature, J. Alloys Compd. 693 (2017) 490–499.
[26] X.W. Li, S.L. Xiong, J.F. Li, J. Bai, Y.T. Qian, Mesoporous NiO ultrathin nanowire networks topotactically transformed from α-$Ni(OH)_2$ hierarchical microspheres and their superior electrochemical capacitance properties and excellent capability for water treatment, J. Mater. Chem. 22 (2012) 14276–14283.
[27] S.T. Ren, C. Yang, C. Sun, Y.H. Hui, Z.J. Dong, J.D. Wang, X.T. Su, Novel NiO nanodisks and hollow nanodisks derived from $Ni(OH)_2$ nanostructures and their catalytic performance in epoxidation of styrene, Mater. Lett. 80 (2012) 23–25.
[28] R. Zamiri, H.A. Ahangar, A. Rebelo, G. Zamiri, A. Zakaria, Hydrothermal synthesis and ESR analysis of NiO dendrite and tree-like nanostructures, Res. Chem. Intermed. 43 (2017) 2881–2888.
[29] Y.J. Zhang, W. Zeng, New insight into gas sensing performance of nanoneedle-assembled and nanosheet-assembled hierarchical NiO nanoflowers, Mater. Lett. 195 (2017) 217–219.
[30] M.J. Dai, L.P. Zhao, H.Y. Gao, P. Sun, F.M. Liu, S.A. Zhang, K. Shimanoe, N. Yamazoe, G.Y. Lu, Hierarchical assembly of α-Fe_2O_3 nanorods on multiwall carbon nanotubes as a high-performance sensing material for gas sensors, ACS Appl, Mater. Interfaces 9 (2017) 8919–8928.
[31] W. Zen, T.M. Liu, Gas-sensing properties of SnO_2-TiO_2-based sensor for volatile organic compound gas and its sensing mechanism, Physica B 405 (2010) 1345–1348.

[32] B.Y. Kim, J.H. Ahn, J.W. Yoon, C.S. Lee, Y.C. Kang, F. Abdel-Hady, A.A. Wazzan, J.H. Lee, Highly selective xylene sensor based on NiO/$NiMoO_4$ nanocomposite hierarchical spheres for indoor air monitoring, ACS Appl. Mater. Interfaces 8 (2016) 34603–34611.
[33] M. Hübner, C.E. Simion, A. Tomescu-Stanoiu, S. Pokhrel, N. Barsan, U. Weimar, Influence of humidity on CO sensing with p-type CuO thick film gas sensors, Sens. Actuators B 153 (2011) 347–353.
[34] F. Li, Q.X. Qin, N. Zhang, C. Chen, L. Sun, X. Liu, Y. Chen, C.N. Li, S.P. Ruan, Improved gas sensing performance with Pd-doped $WO_3 \cdot H_2O$ nanomaterials for the detection of xylene, Sens. Actuators B 244 (2017) 837–848.
[35] Y.J. Li, X.H. Ma, S.J. Guo, B. Wang, D.M. Sun, X.D. Zhang, S.P. Ruan, Hydrothermal synthesis and enhanced xylene-sensing properties of pompon-like Cr-doped Co_3O_4 hierarchical nanostructures, RSC Adv. 6 (2016) 22889–22895.
[36] R.L. Xu, N. Zhang, L. Sun, C. Chen, Y. Chen, C.N. Li, S.P. Ruan, One-step synthesis and the enhanced xylene-sensing properties of Fe-doped MoO_3 nanobelts, RSC Adv. 6 (2016) 106364–106369.
[37] L.L. Sui, X.F. Zhang, X.L. Cheng, P. Wang, Y.M. Xu, S. Gao, H. Zhao, L.H. Huo, Au-loaded hierarchical MoO_3 hollow spheres with enhanced gas-sensing performance for the detection of BTX (benzene toluene, and xylene) and the sensing mechanism, ACS Appl. Mater. Interfaces 9 (2017) 1661–1670.
[38] D.S. Jiang, W. Wei, F. Li, Y.J. Li, C.X. Liu, D.M. Sun, C.H. Feng, S.P. Ruan, Xylene gas sensor based on α-MoO_3/α-Fe_2O_3 heterostructure with high response and low operating temperature, RSC Adv. 5 (2015) 39442–39448.
[39] L.H. Zhu, D.Z. Zhang, Y. Wang, C.H. Feng, J.R. Zhou, C.X. Liu, S.P. Ruan, Xylene gas sensor based on Ni doped TiO_2 bowl-like submicron particles with enhanced sensing performance, RSC Adv. 5 (2015) 28105–28110.
[40] L. Liu, Z.C. Zhong, Z.J. Wang, L.Y. Wang, S.C. Li, Z. Liu, Y. Han, Y.X. Tian, P.L. Wu, X. Meng, Synthesis characterization, and m-xylene sensing properties of Co-ZnO composite nanofibers, J. Am. Ceram. Soc. 94 (2011) 3437–3441.
[41] C.Q. Ge, C.S. Xie, D.W. Zeng, S.Z. Cai, Formaldehyde- benzene-, and xylene-sensing characterizations of Zn-W-O nanocomposite ceramics, J. Am. Ceram. Soc. 90 (2007) 3263–3267.
[42] J.H. Kim, H.M. Jeong, C.W. Na, J.W. Yoon, F. Abdel-Hady, A.A. Wazzan, J.H. Lee, Highly selective and sensitive xylene sensors using Cr_2O_3-$ZnCr_2O_4$ hetero-nanostructures prepared by galvanic replacement, Sens. Actuators B 235 (2016) 498–506.
[43] H.J. Kim, J.W. Yoon, K.I. Choi, H.W. Jang, A. Umar, J.H. Lee, Ultraselective and sensitive detection of xylene and toluene for monitoring indoor air pollution using Cr-doped NiO hierarchical nanostructures, Nanoscale 5 (2013) 7066–7073.
[44] C.H. Feng, C. Wang, H. Zhang, X. Li, C. Wang, P.F. Cheng, J. Ma, P. Sun, Y. Gao, H. Zhang, Y.F. Sun, J. Zheng, G.Y. Lu, Enhanced sensitive and selective xylene sensors using W-doped NiO nanotubes, Sens. Actuators B 221 (2015) 1475–1482.
[45] M.E. Franke, T.J. Koplin, U. Simon, Metal and metal oxide nanoparticles in chemiresistors: does the nanoscale matter, Small 2 (2006) 36–50.
[46] N. Rezlescu, C. Doroftei, E. Rezlescu, P.D. Popa, Lithium ferrite for gas sensing applications, Sens. Actuators B 133 (2008) 420–425.
[47] C. Wang, J.Y. Liu, Q.Y. Yang, P. Sun, Y. Gao, F.M. Liu, J. Zheng, G.Y. Lu, Ultrasensitive and low detection limit of acetone gas sensor based on W-doped NiO hierarchical nanostructure, Sens. Actuators B 220 (2015) 59–67.
[48] Y.L. Wang, C. Liu, L. Wang, J. Liu, B. Zhang, Y. Gao, P. Sun, Y.F. Sun, T. Zhang, G.Y. Lu, Horseshoe-shaped SnO_2 with annulus-like mesoporous for ethanol gas sensing application, Sens. Actuators B 240 (2017) 1321–1329.
[49] D. Kohl, Function and applications of gas sensors, J. Phys. D: Appl. Phys. 34 (2001) R125–R149.
[50] M. Yang, H.F. Pu, Q.F. Zhou, Q. Zhang, Transparent p-type conducting K-doped NiO films deposited by pulsed plasma deposition, Thin Solid Films 520 (2012) 5884–5888.
[51] J.W. Yoon, H.J. Kim, I.D. Kim, J.H. Lee, Electronic sensitization of the response to C_2H_5OH of p-type NiO nanofibers by Fe doping, Nanotechnology 24 (2013) 44405–44412.
[52] H.J. Kim, H.M. Jeong, T.H. Kim, J.H. Chung, Y.C. Kang, J.H. Lee, Enhanced ethanol sensing characteristics of In_2O_3-decorated NiO hollow nanostructures via modulation of hole accumulation layers, ACS Appl. Mater. Interfaces 6 (2014) 18197–18204.
[53] C. Wang, X.B. Cui, J.Y. Liu, X. Zhou, X.Y. Cheng, P. Sun, X.L. Hu, X.W. Li, J. Zheng, G.Y. Lu, Design of superior ethanol gas sensor based on Al-doped NiO nanorod-flowers, ACS Sens. 1 (2016) 131–136.
[54] M.R. Alenezi, A.S. Alshammari, K.D.G.I. Jayawardena, M.J. Beliatis, S.J. Henley, S.R.P. Silva, Role of the exposed polar facets in the performance of thermally and UV activated ZnO nanostructured gas sensors, J. Phys. Chem. C 117 (2013) 17850–17858.

Biographies

Hongyu Gao received the BS degree in Department of Electronic Science and Engineering in 2016. He is currently studying for his MS degree in College of Electronic Science and Engineering, Jilin University, China.

Dongdong Wei received the BS degree in Changchun University of Science and Technology in 2016. He is currently studying for his MS degree in College of Electronic Science and Engineering, Jilin University, China.

Pengfei Lin received the BS degree in Department of Electronic Science and Engineering in 2015. He is currently studying for his MS degree in College of Electronic Science and Engineering, Jilin University, China.

Chang Liu received the MS degree in Department of Electronic Sciences and Technology in 2015. Now she is currently working toward the Ph.D degree in the Electronics Science and Engineering department, Jilin University. Her research interests include the synthesis of functional materials and their applications in gas sensors.

Peng Sun received his PhD degree from College of Electronic Science and Engineering, Jilin University, China in 2014. He was appointed the lecturer in Jilin University in the same year. Now, he is engaged in the synthesis and characterization of the semiconducting functional materials and gas sensors.

Kengo Shimanoe has been a professor at Kyushu University since 2005. He received a B. Eng. degree in applied chemistry in 1983 and a M. Eng. degree in 1985 from Kagoshima University and Kyushu University, respectively. He joined Nippon Steel Corp.in1985, and received a Dr. Eng. degree in1993 from Kyushu University. His current research interests include the development of gas sensors and other functional devices.

Noboru Yamazoe had been a professor at Kyushu University since 1981 until he retired in 2004. He received his M. Eng. degree in applied chemistry in 1963 and his Dr. Eng. Degree in 1969 from Kyushu University. His research interests were directed mostly to the development and application of functional inorganic materials.

Geyu Lu received the B.Sci. degree in electronic sciences in 1985 and the M.S. degree in 1988 from Jilin University in China and the Dr. Eng. degree in 1998 from Kyushu University in Japan. Now he is a professor of Jilin University, China. His current research interests include the development of chemical sensors and the application of the function materials.